Biochemistry

 Volume 37, Number 43 October 27, 1998

Articles

Kinetic Analysis and X-ray Structure of Haloalkane Dehalogenase with a Modified Halide-Binding Site†

Geja H. Krooshof,‡ Ivo S. Ridder,§ Armand W. J. W. Tepper,‡ Gerda J. Vos,§ Henriëtte J. Rozeboom,§ Kor H. Kalk,§ Bauke W. Dijkstra,§ and Dick B. Janssen*,‡

Laboratory of Biochemistry and Laboratory of Biophysical Chemistry, BIOSON Research Institute, Groningen Biomolecular Sciences and Biotechnology Institute, University of Groningen, Nijenborgh 4, 9747 AG Groningen, The Netherlands

Received June 26, 1998; Revised Manuscript Received August 24, 1998

ABSTRACT: Haloalkane dehalogenase (DhlA) catalyzes the hydrolysis of haloalkanes via an alkyl−enzyme intermediate. Trp175 forms a halogen/halide-binding site in the active-site cavity together with Trp125. To get more insight in the role of Trp175 in DhlA, we mutated residue 175 and explored the kinetics and X-ray structure of the Trp175Tyr enzyme. The mutagenesis study indicated that an aromatic residue at position 175 is important for the catalytic performance of DhlA. Pre-steady-state kinetic analysis of Trp175Tyr-DhlA showed that the observed 6-fold increase of the K_m for 1,2-dibromoethane (DBE) results from reduced rates of both DBE binding and cleavage of the carbon−bromine bond. Furthermore, the enzyme isomerization preceding bromide release became 4-fold faster in the mutant enzyme. As a result, the rate of hydrolysis of the alkyl−enzyme intermediate became the main determinant of the k_{cat} for DBE, which was 2-fold higher than the wild-type k_{cat}. The X-ray structure of the mutant enzyme at pH 6 showed that the backbone structure of the enzyme remains intact and that the tyrosine side chain lies in the same plane as Trp175 in the wild-type enzyme. The Clα-stabilizing aromatic rings of Tyr175 and Trp125 are 0.7 Å further apart and due to the smaller size of the mutated residue, the volume of the cavity has increased by one-fifth. X-ray structures of mutant and wild-type enzyme at pH 5 demonstrated that the Tyr175 side chain rotated away upon binding of an acetic acid molecule, leaving one of its oxygen atoms hydrogen bonded to the indole nitrogen of Trp125 only. These structural changes indicate a weakened interaction between residue 175 and the halogen atom or halide ion in the active site and help to explain the kinetic changes induced by the Trp175Tyr mutation.

Haloalkane dehalogenase (DhlA)[1] from *Xanthobacter autotrophicus* GJ10 hydrolyzes carbon−halogen bonds in a broad range of haloalkanes, among which are several toxic xenobiotics (*1*). This makes it an interesting enzyme from an environmental point of view. Many details of the catalytic mechanism and structure of DhlA are now well understood (*2*−*7*). The four-step reaction mechanism (Scheme 1) starts with the formation of a Michaelis complex, after which the substrate is covalently bound to the enzyme and a halide ion is cleaved off. Then the alkyl−enzyme intermediate is

† ISR was supported by The Netherlands Foundation for Chemical Research (S. O. N.) with financial aid from The Netherlands Organization for Scientific Research (N. W. O.). GHK and ISR contributed equally to the work reported in this paper.

* To whom correspondence should be addressed at the Department of Biochemistry. Phone: 31-50-3634209. Fax: 31-50-3634165. E-mail: D.B.Janssen@chem.rug.nl.

‡ Laboratory of Biochemistry.

§ Laboratory of Biophysical Chemistry.

[1] Abbreviations: DhlA, haloalkane dehalogenase from *Xanthobacter autotrophicus* GJ10; DBE, 1,2-dibromoethane; DCE, 1,2-dichloroethane; PDB, protein data bank; SDS, sodium dodecyl sulfate; PEG, poly(ethylene glycol).

10.1021/bi9815187 CCC: $15.00
Published on Web 10/02/1998

Scheme 1

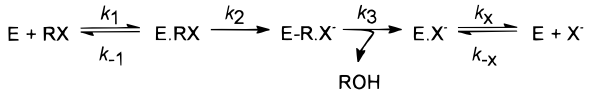

hydrolyzed to produce an alcohol, which is immediately released from the enzyme, and in the final step, the halide ion is removed from the active site. The active site is located in a cavity that is enclosed by the main domain which has an α/β-hydrolase fold structure (*8, 9*), and the cap domain comprising five α-helices (residues 156−229). The main domain provides a scaffold for the catalytic triad residues Asp124, His289, and Asp260, whereas the cap domain influences the substrate specificity (*10*) and is proposed to play a role in halide release (*6*).

The three-dimensional structures of DhlA with substrate and with halide product bound showed that Trp175 and Trp125 form a specific halogen/halide-binding site. The substrate's halogen atom, as well as the negatively charged halide ion, are located in the planes of the aromatic rings, interacting with the hydrogen atoms of the ring nitrogen atoms (*3, 11*). Analysis of several mutants at position 125 or 175 indicated that both residues are involved in transition-state stabilization during formation of the covalent intermediate (*12*). Moreover, Trp175 is located in an N-terminal helix-loop-helix structure (residues 159−181) in the cap domain that covers the catalytic site and that was proposed to be involved in the kinetically observed enzyme isomerization occurring before the actual halide release (*13*).

To obtain more insight in the structural and functional role of Trp175 in haloalkane dehalogenase, we analyzed several haloalkane dehalogenases with mutations at position 175 and studied the X-ray structure and steady-state and pre-steady-state kinetics of the Trp175Tyr enzyme. Trp175 was substituted by a phenylalanine, tyrosine, histidine, arginine, and glutamine, the latter of which was made in a previous study (*12*). Glutamine and arginine were chosen to check the importance of an aromatic residue at position 175 for its interactions with Phe190, Trp194, and the halide ion. Phenylalanine, tyrosine, and histidine were selected to investigate the importance of the indole nitrogen, while retaining aromaticity. The phenylalanine was also picked because it is located in the modeled structure of the dehalogenase isolated from *Sphingomonas paucimobilis* UT26 at the same position as Trp175 in DhlA (*14*).

MATERIALS AND METHODS

Materials. Restriction enzymes, Klenow enzyme, T4-ligase, and isopropyl β-D-thiogalactopyranoside (IPTG) were obtained from Boehringer Mannheim. Bacteriophage R408, T7 polymerase, and DNA sequencing reagents were obtained from Pharmacia LKB Biotechnology. Monodeoxyribonucleoside 5′-triphosphates (dNTPs) were purchased from Promega, [α-^{35}S]dATP was from Amersham Lifescience, and the oligonucleotides for site-directed mutagenesis and sequencing were synthesized by Eurosequence (Groningen, The Netherlands). Halogenated compounds were obtained from Janssen Chimica or from Merck. ^2H_2O (99.8% v/v) was purchased from Merck or from Isotec Inc.

Bacterial Strains and Plasmids. Escherichia coli JM101 (Promega) was used for standard DNA manipulations and the production of single-stranded DNA for sequencing, while uracil-containing single-stranded DNA for site-directed mutagenesis was produced by *E. coli* BW313 (*15*). *E. coli* strain BL21(DE3) (*16*) was used to overproduce mutant haloalkane dehalogenases.

The mutagenesis and expression vector pGELAF+ was used to construct the Trp175 mutants of haloalkane dehalogenase. This plasmid carries the wild-type dehalogenase gene (*dhlA*) under the control of the phage T7 promoter (*17*).

Site-Directed Mutagenesis. All standard molecular DNA techniques were performed as described by Sambrook et al. (*18*). Mutants of haloalkane dehalogenase were constructed according to the Kunkel method (*15*). The general mutagenic primer used was 5′-GCCTGCAGATGGCTTTACCGCC-**XXX**AAATACGAT-3′, in which the introduced *Pst*I restriction site is shown underlined and the codon of amino acid 175 is indicated in boldface type. The codons TAC, TTC, CAC, and CGC were used to change Trp175 to Tyr, Phe, His, and Arg, respectively. pGELAF+ was used as a template, and transformants were screened for an additional *Pst*I restriction site. DNA sequences were verified by the dideoxy chain-termination method (*19*).

Protein Expression and Purification. Expression and purification of the dehalogenase enzymes involved chromatography on DEAE cellulose and hydroxylapatite as described earlier by Schanstra et al. (*17*). The enzymes were concentrated with an Amicon ultrafiltration cell using a PM30 filter and stored at −20 or 4 °C in TEMAG [10 mM Tris-sulfate, pH 7.5, 1 mM EDTA, 1 mM 2-mercaptoethanol, 3 mM sodium azide, and 10% (v/v) glycerol]. Coomassie brilliant blue was used to determine protein concentrations of crude extracts with bovine serum albumin as a standard. The concentrations of purified enzyme were measured by its absorbance at 280 nm using the absorbance coefficient $\epsilon_{280} = 4.87 \times 10^4\ M^{-1}cm^{-1}$. The purity of the isolated enzymes was analyzed by SDS−polyacrylamide gel electrophoresis.

Steady-State Kinetics. Dehalogenase assays were carried out using colorimetric detection of halide release (*1*). Solvent kinetic isotope effects were determined by performing dehalogenase assays in buffers containing ^2H_2O concentrations ranging 0−90%. The K_m, V_{max}, and k_{cat}/K_m were calculated from the alcohol and halide production rates at pH 8.2 and 30 °C, which were measured using colorimetric assays and gas chromatography, as described previously by Krooshof et al. (*20*).

Stopped-Flow Experiments. Stopped-flow fluorescence quenching experiments were performed to determine the pre-steady-state kinetics of halide and substrate binding and steady-state halide dissociation constants (K_d). All measurements were carried out on an Applied Photophysics SX17MV stopped-flow instrument. The reactions were performed in TEMAG buffer (pH 8.2) at 30 °C and the reported reactant concentrations are those in the reaction chamber after mixing. The excitation wavelength was set at 290 nm, and the emission was monitored above 320 nm using a cutoff filter. Each fluorescence trace shown is the average of four individual experiments.

Rapid-Quench Experiments. Rapid-quench measurements were performed in TED buffer (50 mM Tris-SO_4, pH 8.2, 1 mM EDTA, and 1 mM dithiotreitol) at 30 °C using an RQF-63 rapid-quench instrument from KinTek Corporation. A

reaction was initiated by mixing equal volumes (50 μL) of protein and substrate, and quenched with 0.3 M H_2SO_4 (end concentration) after appropriate time intervals (5 ms to 2 s). Immediately after quenching, the reaction mixture was thoroughly extracted with 1.5 mL of ice-cold diethyl ether, containing 0.05 mM 1-bromohexane as the internal standard. The diethyl ether phase containing noncovalently bound substrate and the alcohol produced was neutralized by addition of H_2CO_3 and analyzed by gas chromatography as described for the K_m determinations. In all cases, the enzyme and substrate concentrations cited in the text are those after mixing and during the enzymatic reaction.

Data Analysis. Apparent steady-state dissociation constants (K_d) for halide binding to DhlA were determined from the steady-state part of the stopped-flow fluorescence traces. The calculations involved nonlinear regression fitting (SigmaPlot, Jandel Scientific) using the equation $(F_0 - F)/F_0 = (f_a[X^-])/([X^-] + K_d)$, where F is the observed fluorescence at halide concentration $[X^-]$, K_d is the apparent dissociation constant, and f_a is the fraction of the total fluorescence that is quenched at $[X^-] \gg K_d$.

Nonlinear least-squares analysis of the primary stopped-flow fluorescence data was performed using the software provided with the instrument. All fluorescence data obtained from halide and substrate binding experiments could be described by the single-exponential equation $F = \beta + \alpha e^{-k_{obs}t}$, in which β is the end level of the fluorescence signal, α is the amplitude, and k_{obs} is the observed rate. These kinetic parameters were further used to derive a binding mechanism with accompanying microscopic rate and equilibrium constants.

Rates and equilibrium constants for substrate conversion were derived from rapid-quench data by numerical simulation of Scheme 1, using the computer program Scientist (Micromath). The fits were constrained by the experimentally determined steady-state k_{cat} and K_m values and by the fact that k_{cat}/K_m sets the lower limit for k_1 (*21*). The Scientist output was analyzed with the spreadsheet program Quattro-Pro (Borland International) to check whether the numerical simulations agreed with the experimental data. Under initial velocity steady-state conditions, $k_{cat} = (k_2k_3k_x)/(k_2k_3 + k_2k_x + k_3k_x)$, $K_m = [k_3k_x(k_{-1} + k_2)]/[k_1(k_2k_3 + k_2k_x + k_3k_x)$, and $(k_{cat}/K_m) = (k_1k_2)/(k_{-1} + k_2)$. These equations hold for Scheme 1 and were derived using the determinant method described by Huang (*22*).

Crystallization of Trp175Tyr Haloalkane Dehalogenase and Soaking Experiments. The dehalogenase mutant Trp175Tyr was subjected to crystallization experiments at room temperature using the vapor diffusion method in hanging drop setups. The drops consisted of 4 μL of 5.5 mg/mL protein in 100 mM MES [2-(*N*-morpholino)ethanesulfonic acid] buffer, pH 5.6, mixed with an equal volume of reservoir solution. Ammonium sulfate was used as a precipitant in the concentration range 44−58% saturation (at 0 °C) in 100 mM MES buffer (pH 5.6−6.0). Crystals were obtained within a week from 50% $(NH_4)_2SO_4$ in 100 mM MES buffer (pH 5.6). The crystals are lozenge shaped and belong to the orthorhombic space group $P2_12_12$, with cell axes $a = 95.2$ Å, $b = 73.0$ Å, and $c = 41.5$ Å. This is very similar to the conditions and parameters for the wild-type crystals (*23*).

In a soaking experiment, several crystals were immersed in a solution of 50% $(NH_4)_2SO_4$ in 100 mM acetate buffer (pH 5.0) for about 2−3 h at room temperature. Wild-type DhlA crystals were subjected to the same conditions.

Diffraction Data Collection. Three diffraction experiments were carried out in total. One data set was collected from one single crystal of Trp175Tyr-DhlA at pH 6.0 at room temperature on an Enraf Nonius FAST area detector system (Enraf Nonius, Delft, The Netherlands). The detector was equipped with a CAD4 κ-goniostat and received graphite monochromatized CuKα radiation ($\lambda = 1.5418$ Å) from an Elliot GX21 rotating anode X-ray generator. Data were collected and processed with the MADNES package (*24*). Profile fitting and local scaling of the data was done according to Kabsch (*25*), after which the data were merged with the in-house BIOMOL crystallographic package (Protein Crystallography Group, University of Groningen).

In the same setup, a data set was collected at 120 K from a mutant enzyme crystal soaked at pH 5.0. A solution of 30% (w/v) PEG 6000, 20% (v/v) glycerol, and 100 mM acetate buffer (pH 5.0) was applied as a cryoprotectant. Likewise, a data set was collected at cryo temperature from a wild-type enzyme crystal soaked in the same pH 5.0 mother liquor. Further information on the data processing is given in Table 1.

Structure Solution and Crystallographic Refinement. The room-temperature structure was solved by positioning the structure of the wild-type DhlA at pH 6.2 [PDB entry 2HAD (*2*)] with Trp175 replaced by Ala as a model in the mutant cell. Atomic *B*-factors were taken from the wild-type structure and kept constant during the refinement because of the limited resolution. The model was refined with X-PLOR versions 3.1 and 3.843 (*26*). A random set of 5% of the unique reflections was set apart to calculate R_{free} values (*27*) as an independent validation of the refinement progress. First, a rigid body refinement was done to position the molecule more precisely in the asymmetric unit. This led to a significant drop in R_{free} from 30.2 to 25.7% (data from 8 to 4 Å resolution). Then several rounds of positional refinement were applied using data from 8 to 2.6 Å. An OMIT $F_o - F_c$ electron density map (*28*, *29*) calculated at this stage clearly showed density for a tyrosine at the 175 position. This side chain was then extended to tyrosine and water molecules were included only at positions where the wild-type DhlA contained solvent molecules as well. This was followed by several more cycles of positional refinement, making use of a bulk-solvent mask in X-PLOR (data 20−2.6 Å). A final cycle of positional refinement including all data was used to make some final corrections. At all stages, OMIT $2F_o - F_c$ and $F_o - F_c$ electron density maps were calculated and inspected with O (*30*) to check the agreement of the model with the data. PROCHECK (*31*) and WHATCHECK (*32*) were used to assess the stereochemical quality. Whenever necessary the model was manually adjusted with O. The refinement was stopped when it gave no further decrease in R_{free} or improvement in stereochemistry.

The resulting structure was used as a starting model in the refinement of the pH 5.0 structures of both mutant and wild-type enzyme. The set of reflections that was set apart to calculate R_{free} values in the room-temperature structure refinement was extended to cover 5% of the additional

Table 1: Statistics of Data Collection and Quality of the Final Models of Trp175Tyr and Wild-Type Haloalkane Dehalogenase

	Trp175Tyr-DhlA pH 6.0	Trp175Tyr-DhlA pH 5.0	wild-type DhlA pH 5.0
cell dimensions (Å)	$a = 95.2$, $b = 73.0$, $c = 41.5$	$a = 93.1$, $b = 72.3$, $c = 41.1$	$a = 92.6$, $b = 72.5$, $c = 41.4$
resolution range (Å) (highest resolution shell)	32−2.60 (2.67−2.60)	31−2.10 (2.13−2.10)	31−1.96 (2.00−1.96)
no. of observations	13 050	65 239	56 912
no. of unique reflections	7742	13 700	18 082
completeness (%) (highest resolution shell)	82.6 (80.8)	79.0 (60.5)	87.2 (42.3)
$\langle I/\sigma(I)\rangle$	8.6	13.6	10.5
R_{merge} (%)[a] (highest resolution shell)	8.1 (27.7)	7.5 (13.6)	7.3 (19.1)
R_{iso} (%)[b] (highest resolution shell)	14.3 (27.6)	28.2 (39.9)	27.9 (35.0)
	Quality of the Final Model		
no. of atoms			
protein	2476	2476	2478
acetic acid		8	8
solvent	82	279	319
final *R*-factor (%)	19.3 (20−2.6 Å, all data)	17.1 (20−2.1 Å, all data)	16.9 (20−1.96 Å, all data)
free *R*-factor (%)	25.3 (20−2.6 Å, test set)	22.5 (20−2.1 Å, test set)	22.0 (20−1.96 Å, test set)
rmsd from ideality			
bond lengths (Å)	0.007	0.008	0.008
bond angles (deg)	1.4	1.5	1.5
dihedrals (deg)	23.6	23.4	23.4
impropers (deg)	1.2	1.2	1.2
ΔB for bonded atoms		1.4 Å^2	1.3 Å^2
$<B>$ overall (Å^2)		14.1	11.6
$<B>$ protein (Å^2)		13.0	10.2
$<B>$ acetic acid active site		29.0 Å^2	15.8 Å^2
est. coordinate error (Å)[c]	0.29	0.19	0.17

[a] R_{merge} (%) $= \sum_{hkl}\sum_{refl}|I(hkl, j) - \langle I(hkl)\rangle|/\sum_{hkl}\sum_{refl}\langle I(hkl)\rangle$. [b] R_{iso} (%) $= \sum_{hkl}|F(hkl, \text{other}) - F(hkl, \text{native})|/\sum_{hkl}F(hkl, \text{native})$. [c] Derived from a σ_A plot (*43*).

reflections as well. The models were refined with X-PLOR version 3.843. The molecule was positioned in the smaller cell by rigid body refinement and the tryptophan was reintroduced at the 175 position for the wild-type structure. This was followed by several cycles of positional and *B*-factor refinement, making use of a bulk-solvent mask in X-PLOR (data beyond 20 Å). In both cases, the refinement was completed by a cycle including all data. The same structure validation strategy as described above was applied throughout the refinement. The atomic coordinates and structure factor amplitudes for all three structures have been deposited in the Brookhaven Protein Data Bank with the entry codes 1bee, 1bez, and 1be0, respectively.

RESULTS

Site-Directed Mutagenesis and Specific Activities. Trp175 in haloalkane dehalogenase (DhlA) was mutated to tyrosine, phenylalanine, histidine, and arginine using the Kunkel method. The mutated enzymes were all expressed at 17 °C as soluble protein in quantities similar to wild-type enzyme. The specific activities of these mutants measured in crude extracts with 1,2-dichloroethane (DCE) and 1,2-dibromoethane (DBE) are listed in Table 2 and show that DBE activity increases in the order Arg < Gln < His < Phe < Tyr ≈ Trp (wild-type residue). Only the tyrosine mutant displayed no reduction in activity for DBE. DCE could only be hydrolyzed by the DhlA mutants Trp175Phe and Trp175Tyr, although 10- and 15-fold slower compared to the wild-type enzyme, respectively. From these results, it is obvious that an aromatic residue at position 175 is important for the catalytic performance of haloalkane dehalogenase. The DhlA mutant Trp175Tyr was selected for further kinetic and structural analysis.

Table 2: Specific Activities of Wild-Type and Mutant Haloalkane Dehalogenases in Cell-Free Extracts[a]

	DBE[b] (units/mg)	DCE[b] (units/mg)
wild-type	2.3	2.9
Trp175Tyr	2.5	0.14
Trp175Phe	0.47	0.28
Trp175His	0.24	–
Trp175Arg	–[c]	–
Trp175Gln	0.15	–

[a] The crude extracts were produced from late-exponential, induced cultures grown at 17 °C. The expression levels ranged 30−60% of the total protein contents of cell-free extract. [b] Substrate solutions contained 5 mM 1,2-dibromoethane (DBE) or 30 mM 1,2-dichloroethane (DCE), respectively. [c] (−) not detectable (<25 milliunits/mg).

Table 3: Halide-Binding and Steady-State Activity Parameters of Purified Wild-Type and Trp175Tyr Haloalkane Dehalogenase for DBE and DCE at pH 8.2 and 30 °C

	K_m (mM)	k_{cat} (s^{-1})	k_{cat}/K_m (mM^{-1} s^{-1})	K_d (mM)	f_a	k_H/k_D[a]
1,2-dibromoethane						
wild-type[b]	0.01	3.0	300	10	0.34	2
Trp175Tyr	0.06	5.0	85	137	0.10	2
1,2-dichloroethane						
wild-type	0.53	3.3	6.2	75	0.31	2
Trp175Tyr	2.85	0.33	0.1	>1000	0.10	1

[a] Solvent (D_2O) kinetic isotope effect on dehalogenase activity. k_H and k_D are the k_{cat} values determined in H_2O and 90% D_2O, respectively. [b] Taken from Schanstra et al. (*7*).

Steady-State Kinetics and Halide Binding of Trp175Tyr Haloalkane Dehalogenase. Steady-state kinetic parameters were determined using purified Trp175Tyr-DhlA with DBE or DCE as the substrates (Table 3). Although this mutant shows a 2-fold higher conversion rate (k_{cat}) for DBE than wild-type DhlA, its catalytic efficiency toward this substrate

is lower, because of an increase of K_m. In the case of DCE, k_{cat} decreased 10-fold and K_m increased 6-fold compared with wild-type values.

A solvent kinetic isotope effect of ^2H_2O was observed on the rate of DBE conversion by Trp175Tyr-DhlA (Table 3), suggesting that either hydrolysis of the alkyl−enzyme intermediate (k_3 in Scheme 1) or bromide release (k_x) is the rate-determining reaction step (*7*). The absence of the isotope effect on the k_{cat} of DCE hydrolysis indicates that in this case the rate-limiting step has shifted to a step before hydrolysis of the covalent intermediate.

Besides a reduced affinity for substrate, the Trp175Tyr mutant also displays a lower affinity for halide ions compared to wild-type enzyme (Table 3). The apparent dissociation constant (K_d) increased 14-fold for bromide ions, while the K_d for chloride ions became too high to be measured accurately by fluorescence quenching experiments. Moreover, the loss of a tryptophan residue in the mutated enzyme resulted in a lower degree of quenching (f_a) (Table 3).

Pre-Steady-State Kinetic Analysis of 1,2-Dibromoethane Conversion by Trp175Tyr-DhlA. A multiple turnover rapid-quench flow experiment with substrate in 30-fold excess over enzyme was performed to establish the rate-determining step in the hydrolysis of DBE by Trp175Tyr-DhlA (Figure 1A). The Trp175Tyr dehalogenase showed a linear production of 2-bromoethanol in time, whereas a burst of 2-bromoethanol production was observed with wild-type DhlA (*7*). The absence of a product burst implies that 2-bromoethanol formation or a step preceding it is the slowest reaction step. Together with the observed kinetic isotope effect we can conclude that hydrolysis of the intermediate must be the slowest step in the Trp175Tyr dehalogenase. Furthermore, Figure 1A clearly indicates that under steady-state conditions (i.e., in the last part of the curve) the mutant dehalogenase produced 2-bromoethanol faster than the wild-type enzyme. The steady-state production rate of 2-bromoethanol was 5.8 s^{-1} for Trp175Tyr-DhlA, which is similar to the k_{cat} derived from steady-state halide production (5.0 s^{-1}, Table 3).

A single-turnover rapid-quench experiment in which enzyme (350 μM) was present in excess over DBE (250 μM) clearly showed that the substrate was consumed much faster than 2-bromoethanol was produced or, in other words, formation of the covalent intermediate was faster than its hydrolysis, resulting in its accumulation (Figure 1B). This consolidates the conclusion that hydrolysis of the intermediate is the rate-limiting step. Furthermore, the higher k_{cat} of the Trp175Tyr dehalogenase compared to the wild-type implies that bromide export, which is the slowest step in wild-type DhlA, became faster in the mutated enzyme.

The rates of the individual reaction steps were determined by numerical simulation of the 4-step reaction mechanism in Scheme 1 using the rapid-quench data and the steady-state parameters k_{cat} and K_m (Table 4, fits in Figure 1, panels A and B). As expected, the slowest step in the conversion of DBE appeared to be hydrolysis of the covalent intermediate (k_3), although the rate is similar to the wild-type value. Furthermore, the rate of DBE binding (k_1) decreased 6-fold compared to wild-type DhlA. Formation of the alkyl−enzyme intermediate (k_2) was at least 2-fold slower than with the wild-type, while the rate of bromide release (k_x) was at least 4-fold higher.

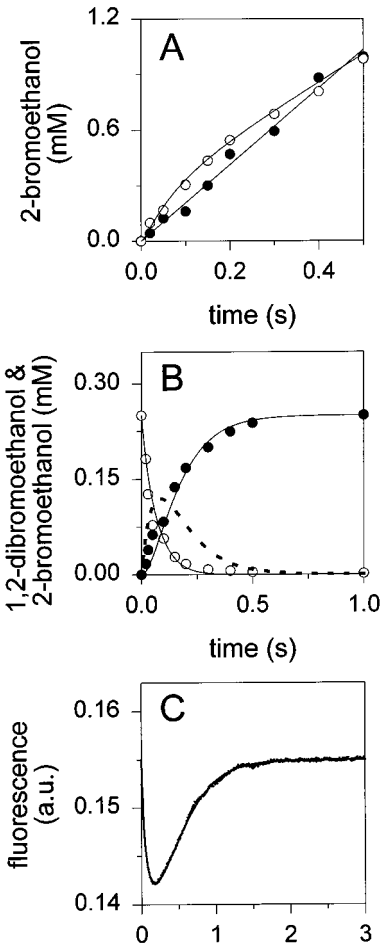

FIGURE 1: Pre-steady-state kinetic analysis of 1,2-dibromoethane (DBE) conversion by Trp175Tyr haloalkane dehalogenase at pH 8.2 and 30 °C. (**A**) Production of 2-bromoethanol during a multiple-turnover rapid-quench experiment of 0.35 mM Trp175Tyr-DhlA (●) or 0.55 mM wild-type DhlA (○) with 10 mM DBE in T_{50}ED buffer. Wild-type data taken from Schanstra et al. (*7*). (**B**) DBE consumption (○) and 2-bromoethanol production (●) in a single-turnover rapid-quench experiment of 0.35 mM dehalogenase with 0.25 mM DBE in T_{50}ED buffer. The solid curves are numerical fits generated by the Scientist program from simulations to Scheme 1. The dotted line represents the simulated concentration of the alkyl−enzyme intermediate in time. (**C**) Single-turnover stopped-flow fluorescence transient obtained after mixing 155 μM enzyme and 120 μM DBE (end concentrations). The solid line is produced by simulation of Scheme 1 with the rate and equilibrium constants mentioned in Table 4 and a fluorescence of 0.7 for the Michaelis complex, 0.75 for the alkyl−enzyme intermediate, and 0.9 for the enzyme−bromide complex in relation to free enzyme.

The rate constants derived from single-turnover rapid-quench experiments could also be used to simulate single-turnover stopped-flow fluorescence data (Figure 1C). The relative fluorescence of the Michaelis complex (E·RX), bromide-bound alkyl−enzyme intermediate (E−R·X^-), and enzyme-bromide complex (E·X^-) compared to free enzyme (E) had to be set at 0.7, 0.75, and 0.9, respectively, compared to 0.35, 0.55, and 0.66 for the wild-type DhlA. Apparently, DBE and bromide cause less quenching of the fluorescence signal of Trp175Tyr-DhlA than of the wild-type signal, which is in agreement with the loss of a Trp residue that interacts with substrate.

Bromide Binding to Trp175Tyr-DhlA. Pre-steady-state kinetics of bromide binding and release were studied by stopped-flow fluorescence quenching experiments under

Table 4: Pre-Steady-State Kinetic Parameters of Purified Wild-Type and Trp175Tyr Haloalkane Dehalogenase for DBE at pH 8.2 and 30 °C

	k_1 (μM^{-1} s^{-1})	k_{-1} (s^{-1})	k_2 (s^{-1})	k_3 (s^{-1})	k_x (s^{-1})	k_{cat}calc[a] (s^{-1})	k_{cat}exp[b] (s^{-1})	$K_m$calc[a] (μM)	$K_m$exp[b] (μM)
wild type[c]	0.75 ± 0.1	>20	>130	10 ± 2	4 ± 1.5	2.8	3	5.6	10
Trp175Tyr	0.12 ± 0.05	30 ± 6	70 ± 15	8 ± 0.7	16 ± 2	5.0	5.8	59	60

[a] Calculated from the rate constants given; for equations, see text. [b] Parameters obtained from steady-state experiments. [c] Taken from Schanstra et al. (*7*).

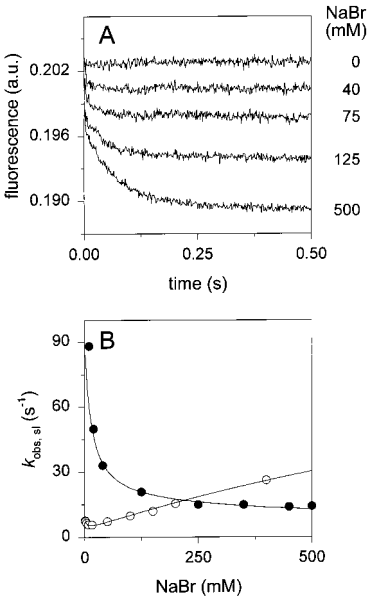

FIGURE 2: Kinetics of bromide binding to Trp175Tyr haloalkane dehalogenase, analyzed by stopped-flow fluorescence quenching. (**A**) Fluorescence transients observed after mixing 7.5 μM enzyme with 0, 40, 75, 125, and 500 mM NaBr in T_{50}EMAG buffer, pH 8.2, at 30 °C (end concentrations). Each trace displays two distinct phases of fluorescence decrease; an initial fast phase followed by a slow phase, the latter of which fitted a single-exponential equation with an observed rate constant $k_{obs,sl}$. (**B**) Observed rate constant $k_{obs,\ sl}$ plotted as a function of the bromide concentration (●). The solid line is the fit obtained by simulation of a three-step mechanism as depicted in Figure 3, upper route. (○) wild-type DhlA data taken from Schanstra and Janssen (*6*).

pseudo-first-order conditions. Figure 2A shows fluorescence transients obtained after rapid mixing of Trp175Tyr dehalogenase (7.5 μM) with various concentrations of NaBr (20−500 mM). Each trace displays an initial burst in fluorescence decrease up to approximately 50% of the total quenching. This large initial decrease is complete within 5 ms and is followed by a slower decline of the fluorescence signal. The fast phases could not be fitted accurately, but every slow phase fitted an exponential, yielding an apparent rate ($k_{obs,sl}$) for each bromide concentration. The $k_{obs,sl}$ decreased with increasing bromide concentrations (Figure 2B). The simplest reaction mechanism that explains both the bromide concentration dependence of $k_{obs,sl}$ and the initial fast fluorescence decrease consists of a rapid bimolecular step preceded and followed by a slow unimolecular isomerization step (Figure 3, upper route). The E_1 species in this mechanism can bind a bromide ion instantaneously, resulting in an immediate quenching of the fluorescence signal. Hence, the initial fluorescence decrease of 50% of the total quenching, which was not observed with wild-type DhlA, implies that about 50% of the enzyme molecules are in the E_1 form in the absence of bromide. All individual rate constants and K_5 could be resolved with an accuracy of 10−20% by numerical simulation and fitting of the fluorescence traces (Figures 2 and 3). The results show that the isomerization steps E → E_1 and EX → E_1X proceed 4−10-fold faster in the Trp175Tyr mutant than in the wild-type dehalogenase, whereas the reverse reaction steps were slowed 10−20-fold. Since the forward and reverse reaction steps have approximately the same rate, about 50% of the Trp175Tyr-DhlA molecules is in the E_1 form in the absence of halide ions, while that was maximally 1% for the wild-type dehalogenase. The calculated apparent dissociation constant (K_d) was in good agreement with the experimentally determined value (Table 3).

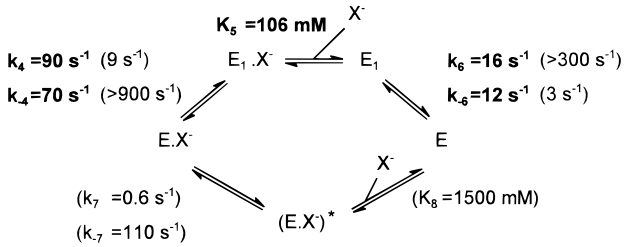

FIGURE 3: Kinetic scheme representing bromide binding and release in wild-type haloalkane dehalogenase (two parallel routes, values between parentheses), and the DhlA mutant Trp175Tyr (upper route only, values in boldface type). The fast equilibrium K_5 equals k_5/k_{-5} with $k_{-5} > 30$ mM^{-1} s^{-1}. The K_d can be calculated by $K_d = [K_5k_4(k_6 + k_{-6})]/[k_{-6}(k_4 + k_{-4})]$.

X-ray Structure of Trp175Tyr-DhlA at pH 6. To study the structural details of the effect of the mutation, we determined the X-ray structure of the Trp175Tyr mutant. The starting model (wild-type dehalogenase at pH 6.2) had to be adjusted only slightly in the course of the crystallographic refinement procedure. In the Trp175Tyr dehalogenase structure, the tyrosine residue at position 175 could be modeled nicely into difference Fourier electron density. After completion of the refinement, the crystallographic *R*-factor was 19.3% for all data between 20 and 2.6 Å. The final model contained one complete molecule of 310 amino acid residues and 82 water molecules at similar positions as in the wild-type model. Like in the wild-type structure, the Ramachandran plot showed two outliers, Asp124 and Asn148, in generously allowed regions. Some parameters indicating the good stereochemical quality of the final model are given in Table 1.

The three-dimensional structure of the mutant enzyme is very similar to the wild-type structure at pH 6.2 and room temperature (*2*). The catalytic triad, formed by residues Asp124, His289, and Asp260, is intact, although the histidine side chain has rotated −22° about χ_2. The other amino acids lining the active-site cavity are in an orientation comparable to that in the wild-type structure. The tyrosine side chain

The high K_m, high K_d, and low f_a of Trp175Tyr-DhlA for DCE and chloride ions made it impossible to study the pre-steady-state kinetics of DCE hydrolysis and chloride binding.

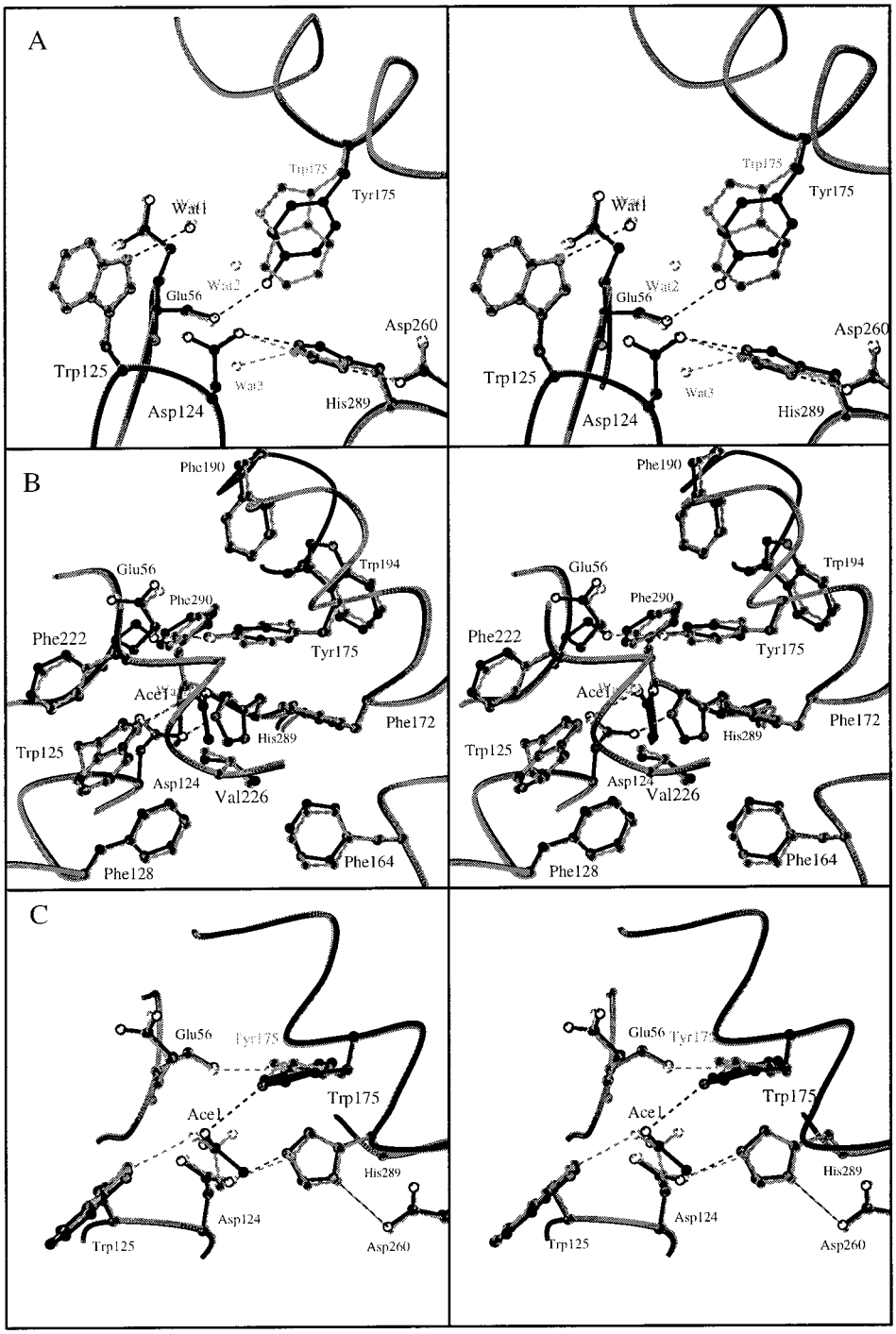

FIGURE 4: Stereoview of the active-site structures of Trp175Tyr and wild-type haloalkane dehalogenase. Relevant residues are drawn as ball-and-stick and parts of the Cα-trace as a coil. All figures are prepared with MOLSCRIPT (*44*). (**A**) Superposition of the active site of Trp175Tyr-DhlA at pH 6 (black lines) and wild-type enzyme at pH 6 (gray lines). Tyr175 in the mutant enzyme is in the same plane as Trp175 in the wild-type structure. Only one water molecule is found in the mutant active site (Wat1), whereas in the wild-type three water molecules (Wat1−3) are depicted, with Wat3 being the activated water molecule. (**B**) Superposition of the active site of Trp175Tyr dehalogenase at pH 5 (black lines) and at pH 6 (gray lines). At pH 5 an acetic acid molecule is bound in the active site with its carbonyl oxygen close to Trp125, while Tyr175 has rotated away. (**C**) Superposition of the active site of wild-type (black lines) and mutant enzyme (gray lines) at pH 5, both of which are complexed with an acetic acid molecule. Tyr175 in the mutant enzyme is further away from the acetic acid carbonyl oxygen than Trp175 in wild-type DhlA, because Tyr175 has rotated away in the mutant.

introduced at position 175 lies in the same plane as Trp175 in the wild-type enzyme, with its aromatic ring partially overlapping the tryptophan pyrrole and phenyl rings (Figure 4A). A short hydrogen bond (2.6 Å) with good geometry is formed between the tyrosine hydroxyl moiety and the Glu56 main chain carbonyl oxygen. The distance between the closest atoms of Trp125 and Trp/Tyr175 has increased from 6.6 to 7.3 Å. The cavity volume as calculated with VOIDOO (*33*) has somewhat increased from 76 to 93 Å^3, mainly as a result of the smaller size of the tyrosine side chain. Inside the cavity, only one water molecule can be identified, whereas there are two present in the wild-type structure. The nucleophilic water molecule is not clearly discernible either. The difference is probably due to the lower resolution of

the Trp175Tyr dehalogenase data.

X-ray Structure of Trp175Tyr-DhlA Containing Acetic Acid at pH 5. The refined structure of the mutant enzyme at pH 5 is very similar to the mutant structure at pH 6 described above. The rms difference of all Cα coordinates is 0.36 Å (0.32 Å when compared to wild-type, pH 6.2), but this difference cannot be attributed to a specific region and is more likely due to the low temperature at which the X-ray data were collected.

Inside the active-site cavity, an acetic acid molecule from the cryoprotectant mother liquor is bound (Figure 4B). One of its oxygen atoms (OXT) lies at the position of a water molecule in the wild-type and mutant pH 6 structures. It is hydrogen bonded to the indole nitrogen of Trp125 only. The other oxygen (O) is at hydrogen-bonding distance from Asp124Oδ1. On the basis of the pK_a difference between acetate and aspartate (4.8 vs 3.9), the acetate is assumed to be bound in the acid form with the proton on the O atom. This atom is also within van der Waals contact distance of the hydroxyl moiety of Tyr175. The acetic acid methyl group is surrounded by an apolar environment (Phe128 and Val226). The average *B*-factor of the molecule is 29.0 Å^2, which is markedly higher than the average *B*-factor of the protein atoms within 5 Å distance from the center of the acetic acid molecule (8.6 Å^2). A second acetic acid molecule is bound at the surface of the protein, close to the N-terminus. Its hydroxyl oxygen is hydrogen bonded to Asp89Oδ1.

As a result of the binding of acetic acid in the active site, several amino acid side chains have changed position in this region. The electron density around the Tyr175 side chain is rather broad in the direction perpendicular to the plane and allows for a range of orientations, varying ca. 35° in χ_2. The predominant orientation of the tyrosine ring is rotated 35° compared to the structure at pH 6 (Figure 4B). Two clusters of interacting aromatic residues surrounding the active-site cavity (Phe222, Trp125, Phe128, Phe164, and Phe172 and Trp194, Phe190, and Phe290) show a small concerted movement of their side chains that enables the Tyr175 side chain to be somewhat flexible. Some of the residues located close to Tyr175 also show broad electron density perpendicular to their rings, permitting variations in χ_2. These movements result in a slightly different shape of the cavity, but the volume is identical to that in the pH 6 structure.

The catalytic triad is intact, and at pH 5, the histidine side chain displays a similar rotation of −16° about χ_2 with respect to the wild-type structure as in the Trp175Tyr pH 6 structure. The hydrolytic water molecule is now clearly discernible in the electron density and occupies the same position close to His289Nε2 and Glu56O as in the wild-type structures.

X-ray Structure of Wild-Type DhlA Containing Acetic Acid at pH 5. For comparison, the wild-type enzyme structure at pH 5 was determined in a similar soaking experiment. The overall structure of DhlA at pH 5 is identical to the mutant structure at this pH and temperature with an rms difference on all Cα coordinates of 0.14 Å. The difference with the wild-type structure at pH 6.2 and room temperature is slightly larger, 0.32 Å, although this difference cannot be ascribed to a defined region of the protein. It is most likely a general effect of the different temperature. Moreover, the active-site region closely resembles that of the wild-type structure at pH 6.2. The amino acid side chains occupy closely identical positions and the volume of the cavity amounts to 75 Å^3. All residues, including the Trp175, are well defined in the electron density.

Like in the mutant enzyme at pH 5, an acetic acid molecule is found inside the cavity in a similar position, but in a somewhat different orientation (Figure 4C). One of its oxygen atoms (OXT) has moved toward the center between the indole nitrogens of Trp125 and Trp175. The other oxygen atom (O) has shifted over 1.3 Å and is now at hydrogen-bonding distance from both carboxylic oxygens of Asp124. Consequently, the methyl group is displaced, too. The average *B*-factor of the molecule is 15.8 Å^2 compared to an overall *B*-factor of 4.4 Å^2 for all atoms within 5 Å distance. This suggests a better defined, stronger binding of the acetic acid molecule to the wild-type enzyme than to the mutant. Another acetate molecule is bound at the surface of the protein at a position different from that in the mutant enzyme described above, with one of its oxygen atoms acting as a hydrogen bond acceptor for Gln10Nε2 and Arg11Nη1.

Acetic Acid as a Substrate Analogue. An acetic acid buffer molecule occupies the active-site cavity in the pH 5 structures of both wild-type and Trp175Tyr-DhlA. We compared these two structures with the structure of DhlA noncovalently complexed with its natural substrate 1,2-dichloroethane [PDB entry 2DHC (*3*)]. Both the acetic acid containing mutant and the wild-type structures are nearly identical to the DCE-bound structure with rmsd values of 0.31 and 0.32 Å for Cα-atoms, respectively, which could be a simple temperature effect. Also the residues lining the active-site cavity can be superimposed on the DCE-bound structure with rmsd values of 0.40 and 0.39 Å for identical atoms, respectively.

When the three structures are superimposed on the basis of all Cα-atoms, the oxygen atom (OXT) of the acetic acid molecule in the mutant and wild-type enzyme is close to the Clα of the DCE molecule at a distance of only 0.7 and 0.6 Å, respectively (Figure 5). The central carbon atom of the acetic acid in both pH 5 structures is in a similar position as the C1 carbon atom of DCE, which undergoes the nucleophilic attack in the second reaction step. The difference in position is 0.6 and 0.5 Å for the mutant and wild-type structure, respectively. The methyl group of the acetic acid molecules is located in the same hydrophobic area of the cavity as the C2 atom of 1,2-dichloroethane. However, the acetic acid molecule differs from DCE in that it contains a protonated oxygen atom that is hydrogen bonded to Asp124 in both wild-type and Trp175Tyr-DhlA, and it obviously lacks the Clβ atom. Nevertheless, the earlier observations suggest that acetic acid can be regarded as a substrate analogue.

Although the binding modes of acetic acid and DCE are very similar in the wild-type enzyme, the binding environment of acetic acid is different in the mutant and wild-type structure. In the wild-type enzyme, the Clα atom of DCE and the oxygen atom of acetic acid are closer to Trp175 than to Trp125, whereas in the mutant, this atom has shifted over 1.3 Å and is now stabilized by Trp125 mainly. In addition, the higher *B*-factors of the acetic acid molecule and its surroundings in the mutant enzyme structure suggest that the binding of substrates is also weaker than that in the wild-type structure.

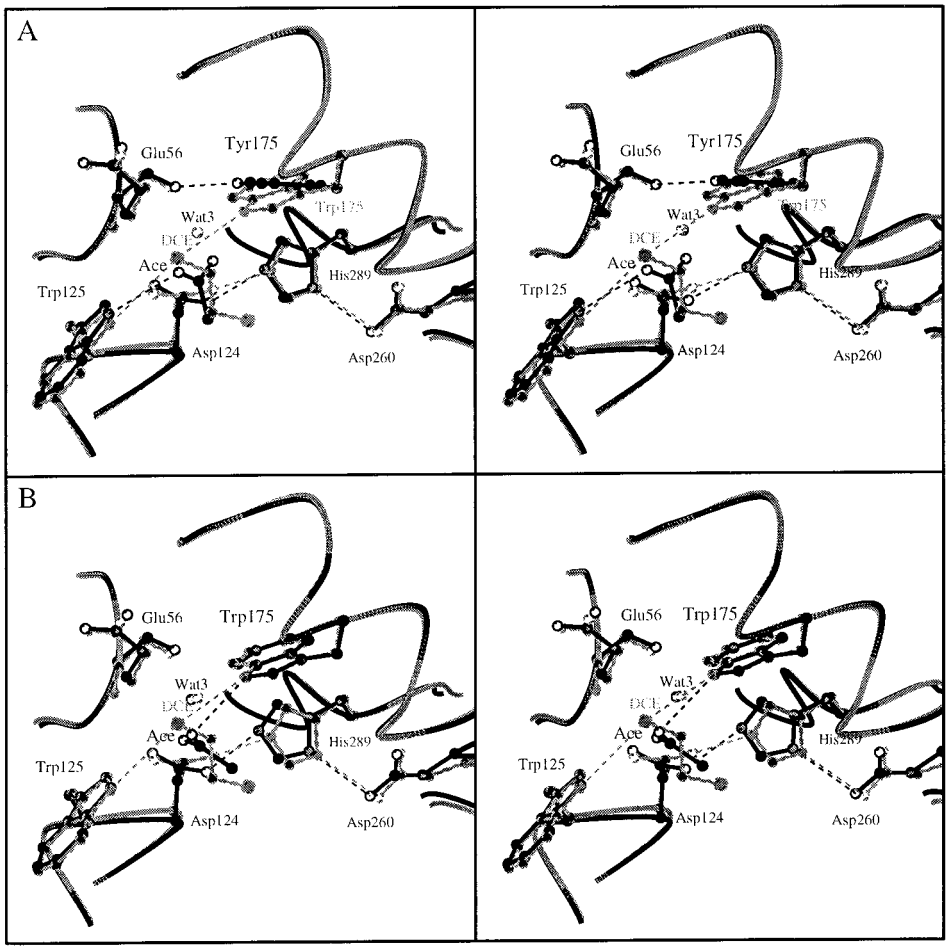

FIGURE 5: Stereoview of the active-site structures of the Trp175Tyr and wild-type DhlA complexed with acetic acid at pH 5 compared to the structure of DhlA complexed with 1,2-dichloroethane (DCE). Relevant residues are drawn as ball-and-stick and parts of the Cα-trace as a coil. The nucleophilic water molecule (Wat3) is depicted as a small sphere. (**A**) Superposition of the active site of the Trp175Tyr mutant−acetic acid complex at pH 5 (black lines) and the wild-type enzyme−DCE complex (gray lines). The acetic acid molecule superimposes nicely on DCE. Its carbonyl oxygen mimics the Clα of DCE, but only shows close van der Waals interactions to Trp125 as Tyr175 has rotated away. In the DhlA−DCE complex, the Clα is in the center between the two tryptophan residues. (**B**) Superposition of the active site of the wild-type enzyme complexed with acetic acid (black lines) and DCE (gray lines). The acetic acid molecule superimposes nicely on DCE and its carbonyl oxygen is closer to Trp175 than to Trp125, in contrast to the mutant.

DISCUSSION

Tryptophan 175 forms a halide-binding site in the active site of DhlA together with Trp125 (*3*, *11*). Upon substrate entrance in the active-site cavity, these residues bind the halogen atom between their indole NH groups and they stabilize the negative charge that develops on the halogen atom during the cleavage of the carbon−halogen bond (*12*, *34*, *35*). Furthermore, Trp175 is part of a helix-loop-helix structure in the cap domain formed by residues 159−181 that was proposed to be involved in a kinetically observed enzyme isomerization occurring before the actual halide release (*13*).

DhlA mutants with Trp175 replaced by Tyr or Phe retain significant activity for both 1,2-dibromoethane and 1,2-dichloroethane, indicating that an aromatic residue at position 175 is important for the catalytic performance of DhlA. Kennes et al. (*12*) concluded the same for residue 125. The preference for aromatic residues at positions 125 and 175 over other halide-stabilizing groups such as guanidinium, amino, or amide groups can be explained by the fact that both residues are involved in aromatic interactions with residues that together form the active site cavity; Trp125 interacts with Phe128 and Phe222, and Trp175 interacts with Phe190 and Trp194. These interactions will be perturbed or lost with aliphatic residues such as Arg and Gln at position 175, resulting in a less well stabilized or organized active-site cavity and halogen/halide-binding site, causing bad transition-state stabilization, and loss of enzyme activity despite the presence of functional groups in their side chains that can interact with the halogen moiety of the substrate.

The structure of the Trp175Tyr dehalogenase mutant at pH 6 showed that the backbone structure of the enzyme has remained intact and that the side chain of Tyr175 lies in the same plane as Trp175 in the wild-type enzyme. Yet, the Trp175Tyr mutation clearly affects the catalytic properties of haloalkane dehalogenase. The conversion rate (k_{cat}) for DBE is 2-fold higher than with the wild-type enzyme and is mainly determined by the rate of hydrolysis of the alkyl−enzyme intermediate (k_3). This step became the slowest reaction step because bromide release became faster in the mutant. Furthermore, the mutant DhlA shows a 6-fold higher K_m for DBE than the wild-type enzyme, which can be ascribed to reduced rates of both DBE binding (k_1) and carbon−bromine cleavage (k_2).

The lower bimolecular rate constant for DBE binding (k_1) is probably accompanied by a lower binding energy of DBE that is caused by loss of the interaction between the Trp175 indole NH and the halogen atom. Also the somewhat larger volume of the cavity and the somewhat wider halogen-binding site between Tyr175 and Trp125 may affect the binding energy.

In the second step of the dehalogenation reaction, a covalent alkyl−enzyme intermediate is formed through a transition state in which a negative charge develops on the halogen atom which is then cleaved off (*3*). This charge is stabilized by the NH atoms of the indole rings of Trp125 and Trp175 in the wild-type enzyme. The X-ray structure of the native enzyme with acetic acid bound shows that this molecule binds in a similar position as the natural substrate 1,2-dichloroethane. Negatively charged groups such as oxygen or sulfur have been observed to interact with the positively charged edge of aromatic rings (*36*−*38*). Therefore, we suggest that acetic acid can be regarded as a substrate analogue. In the Trp175Tyr mutant enzyme, the acetic acid molecule binds to Trp125 only, suggesting that transition-state stabilization in the case of DCE or DBE is achieved predominantly by this residue. This would explain the decrease in k_2 observed in pre-steady-state kinetic experiments with DBE as the substrate.

The same effects can explain the 6-fold increase of the K_m for DCE. The impact on k_2 may be stronger in this case, since chloride is known to be a worse leaving group than bromide. The absence of an isotope effect on the k_{cat} of DCE hydrolysis suggests that k_2 has become the slowest reaction step and may therefore be responsible for the 10-fold decrease in k_{cat} for DCE compared to the wild-type.

It is likely that the Trp175Phe mutation induces similar effects as the Trp175Tyr mutation, since a phenylalanine residue, like tyrosine, is smaller than a tryptophan residue and lacks the indole nitrogen atom too. A phenylalanine residue at position 175 would be even more flexible than a tyrosine, as it would lack the Tyr175OH−Glu56O hydrogen bond. This could explain the observed lower catalytic activities of the Trp175Phe dehalogenase compared to the wild-type activities.

In the third step of the reaction, the covalent alkyl−enzyme intermediate is hydrolyzed by a water molecule that is activated by His289. This water molecule is a hydrogen bond donor to Glu56O, and functions as an acceptor for Gln123Nϵ2 and another water molecule. Although the activated water molecule is present in the crystal structure of the mutant at pH 5, it could not be found in the pH 6 structure, most likely because of the medium resolution of the data. Two components of the hydrolytic machinery show small changes. First of all, the histidine ring has rotated ca. −20° about χ_2. In this orientation, it makes a somewhat more favorable interaction with the hydroxyl moiety of Tyr175, which is positioned in the plane of the histidine ring at 3.8 Å from the Nϵ2 atom. Consequently, the distance between Nϵ2 and the activated water molecule is slightly increased. Furthermore, Glu56O is within hydrogen-bonding distance to the hydroxyl group of Tyr175, which might cause an extra polarization of the C═O bond. However, these are all only minor differences compared to the wild-type situation and do not affect the hydrolysis step in the reaction significantly, as determined by pre-steady-state kinetic measurement.

To complete the catalytic cycle of DhlA, the halide ion is released from the cavity. The dissociation constants of bromide and chloride ions are dramatically affected because of the weaker interactions with the halide ion and the increased rotational flexibility of Tyr175 in the mutant enzyme. The weaker binding of substrate and halide is also reflected in their reduced ability to quench the fluorescence of Trp175Tyr dehalogenase.

Halide release is overall four times faster in Trp175Tyr-DhlA than in the wild-type enzyme. It involves a rapid bimolecular step preceded and followed by a slow unimolecular isomerization step (Figure 3, upper route), which is similar to one of the two wild-type export routes (*6*). The Trp175Tyr mutant either lacks the alternative way of bromide release, or k_{-7} has become slower, making the lower route invisible in the kinetic studies.

The faster bromide release in the Trp175Tyr dehalogenase results from accelerated isomerization steps compared to the wild-type enzyme. The mechanisms associated with the unimolecular steps may involve conformational changes that lead to an "open" enzyme from which the halide ion can readily escape. In the absence of halide ions, less than 1% of the wild-type DhlA molecules is in the "open" E_1 form (*6*), whereas this percentage is approximately 50% for Trp175Tyr-DhlA. This implies that somehow the "open" enzyme conformations (E_1 and $E_1 \cdot X^-$) are more stabilized or the "closed" enzyme forms (E and $E \cdot X^-$) are more destabilized in the mutant enzyme.

Our structural results may provide an explanation for the kinetically observed "open" and "closed" conformations of the enzyme. The increased flexibility of Tyr175 and the occurrence of two main populations of its side chain conformation suggest that residue 175 is closely involved. It is conceivable that in the "closed" conformation the aromatic rings of Trp125 and Trp175 lie in one plane ready to bind the halogen atom or halide ion, whereas during isomerization to the "open" form the interaction of the halide ion with either residue 175 or 125 is lost. A movement of Tyr175 could be an important step in the slow enzyme isomerization that was proposed to involve the helix-loop-helix structure formed by residues 159−181 (*13*). This protein region covers the catalytic site and includes residue 175. A weaker interaction between residue 175 or 125 and the halide ion will increase the rate of the conformational change, which was indeed found in Trp175Tyr-DhlA. Additional information about this step could come from, e.g., NMR experiments (*39*, *40*), time-resolved fluorescence with or without Trp-labeling (*41*), or energy transfer measurements to map distances between certain residues in the cap and main domain in the presence and absence of substrate or halide ions (*42*).

REFERENCES

1. Keuning, S., Janssen, D. B., and Witholt, B. (1985) *J. Bacteriol. 163*, 635−639.
2. Verschueren, K. H. G., Franken, S. M., Rozeboom, H. J., Kalk, K. H., and Dijkstra, B. W. (1993) *J. Mol. Biol. 232*, 856−872.
3. Verschueren, K. H. G., Seljée, F., Rozeboom, H. J., Kalk, K. H., and Dijkstra, B. W. (1993) *Nature 363*, 693−698.

4. Pries, F., Kingma, J., Pentenga, M., van Pouderoyen, G., Jeronimus-Stratingh, C. M., Bruins, A. P., and Janssen, D. B. (1994) *Biochemistry 33*, 1242−1247.
5. Pries, F., Kingma, J., Krooshof, G. H., Jeronimus-Stratingh, C. M., Bruins, A. P., and Janssen, D. B. (1995) *J. Biol. Chem. 270*, 10405−10411.
6. Schanstra, J. P., and Janssen, D. B. (1996) *Biochemistry 35*, 5624−5632.
7. Schanstra, J. P., Kingma J., and Janssen, D. B. (1996) *J. Biol. Chem. 271*, 14747−14753.
8. Franken, S. M., Rozeboom, H. J. Kalk, K. H., and Dijkstra, B. W. (1991) *EMBO J. 10*, 1297−1302.
9. Ollis, D. L., Cheah, E., Cygler, M., Dijkstra, B. W., Frolow, F., Franken, S. M., Haral, M., Remington, S. J., Silman, I., Schrag, J., Sussman, J. L., Verschueren, K. H. G., and Goldman, A. (1992) *Protein Eng. 5*, 197−211.
10. Pries, F., van den Wijngaard, A. J., Bos, R., Pentenga, M., and Janssen, D. B. (1994) *J. Biol. Chem. 269*, 17490−17494.
11. Verschueren, K. H. G., Kingma, J., Rozeboom, H. J., Kalk, K. H., Janssen, D. B., and Dijkstra, B. W. (1993) *Biochemistry 32*, 9031−9037.
12. Kennes, C., Pries, F., Krooshof, G. H., Bokma, E., Kingma, J., and Janssen, D. B. (1995) *Eur. J. Biochem. 228*, 403−407.
13. Schanstra, J. P., Ridder, I. S., Heimeriks, G. J., Rink, R., Poelarends, G. J., Kalk, K. H., Dijkstra, B. W., and Janssen, D. B. (1996) *Biochemistry 35*, 13186−13195.
14. Damborský, J., Bull, A. T., and Hardman, D. J. (1995) *Biologia 50*, 523−528.
15. Kunkel, T. A. (1985) *Proc. Natl. Acad. Sci. U.S.A. 82*, 488−492.
16. Studier, F. W., Rosenberg, A. H., Dunn, J. J., and Dubendorff, J. W. (1990) *Methods Enzymol. 185*, 60−89.
17. Schanstra, J. P., Rink, R., Pries, F., and Janssen, D. B. (1993) *Protein Expression Purif. 4*, 479−489.
18. Sambrook, J., Fritsch, E. F., and Maniatis, T. (1989) *Molecular Cloning: A Laboratory Manual*, Cold Spring Harbor Laboratory Press, Plainview, NY.
19. Sanger, F., Nicklen, S., and Coulsen, A. R. (1977) *Proc. Natl. Acad. Sci. U.S.A. 74*, 5463−5467.
20. Krooshof, G. H., Kwant, E. M., Damborský, J., Koča, J., and Janssen, D. B. (1997) *Biochemistry 36*, 9571−9580.
21. Fersht, A. R. (1985) *Enzyme Structure and Mechanism*, W. H. Freeman and Company, New York.
22. Huang, C. Y. (1979) *Methods Enzymol. 63*, 54−84.
23. Rozeboom, H. J., Kingma, J., Janssen, D. B., and Dijkstra, B. W. (1988) *J. Mol. Biol. 200*, 611−612.
24. Messerschmidt, A., and Pflugrath, J. W. (1987) *J. Appl. Crystallogr. 20*, 306−315.
25. Kabsch, W. (1988) *J. Appl. Crystallogr. 21*, 916−924.
26. Brünger, A. T. (1992) *X-PLOR: A system for X-ray crystallography and NMR, version 3.1*, Yale University Press, New Haven, Connecticut.
27. Brünger, A. T. (1992) *Nature 355*, 472−475.
28. Bhat, T. N. (1988) *J. Appl. Crystallogr. 21*, 279−281.
29. Vellieux, F. M. D., and Dijkstra, B. W. (1997) *J. Appl. Crystallogr. 30*, 396−399.
30. Jones, T. A., Zou, J.-Y., Cowan, S. W., and Kjeldgaard, M. (1991) *Acta Crystallogr., Sect. A 47*, 110−119.
31. Laskowski, R. A., MacArthur, M. W., Moss, D. S., and Thornton, J. M. (1993) *J. Appl. Crystallogr. 26*, 283−291.
32. Vriend, G. (1990) *J. Mol. Graphics 8*, 52−56.
33. Kleywegt, G. J., and Jones, T. A. (1994) *Acta Crystallogr., Sect. D 50*, 178−185.
34. Damborský, J., Kutý, M., Němec, M., and Koča, J. (1997) *JCICS 37*, 562−568.
35. Lightstone, F. C., Zheng, Y.-J., Maulitz, A. H., and Bruice, T. C. (1997) *Proc. Natl. Acad. Sci. U.S.A. 95*, 8417−8420.
36. Thomas, K. A., Smith, G. M., Thomas, T. B., and Feldmann, R. J. (1982) *Proc. Natl. Acad. Sci. U.S.A. 79*, 4843−4847.
37. Reid, K. S. C., Lindley, P. F., and Thornton, J. M. (1985) *FEBS Lett. 190*, 209−213.
38. Burley, S. K., and Petsko, G. A. (1988) *Adv. Protein Chem. 39*, 125−192.
39. Williams, J. C., and McDermott, A. E. (1995) *Biochemistry 34*, 8309−8319.
40. Bizouarn, T., Diggle, C., Quirk, P. G., Grimley, R. L., Cotton, N. P. J., Thomas, C. M., and Jackson, J. B. (1996) *J. Biol. Chem. 271*, 10103−10108.
41. Yamashita, S,. Nishimoto, E,. Szabo, A. G., and Yamasaki, N. (1996) *Biochemistry 35*, 531−537.
42. Bilderback, T., Fulmer, T., Mantulin, W. W., and Glaser, M. (1996) *Biochemistry 35*, 6100−6106.
43. Read, R. J. (1986) *Acta Crystallogr., Sect. A 42*, 140−149.
44. Kraulis, P. (1991) *J. Appl. Crystallogr. 24*, 946−950.

BI9815187